Optimization of spot-size converter for low polarization dependent loss of waveguide photodetector

Joong-Seon Choe,* Won-Seok Han, Duk Jun Kim, Jong-Hoi Kim, Chun Ju Youn, Dong-Young Kim, Yong-Hwan Kwon, and Eun-Soo Nam

Electronics and Telecommunications Research Institute, 218 Gajeong-no, Yuseong-gu, Daejeon 305-700, South Korea

* *jschoe@etri.re.kr*

Abstract: We present an optimization of spot-size converter (SSC) of waveguide photodetector (PD) for small polarization dependent loss (PDL). Beam-propagation method simulation gives responsivity for each polarization and SSC structure. From the calculated responsivity data, optimum structure of SSC is determined that can be implemented with a sufficient process tolerance. We confirm the optimization by measuring PDL of waveguide PD designed according to the structure obtained through the simulation.

OCIS codes: (130.0250) Optoelectronics; (230.5160) Photodetectors; (260.5430) Polarization.

References and links

1. OIF, "Implementation agreements for integrated dual polarization intradyne coherent receivers," (2011).
2. J. Choe, K. Kim, S. Park, J. Kim, J. Lee, M. Kim, S. Park, and J. Ju, "A spot-size converter-integrated 1.3 μm TM mode LD for coupling with surface-plasmon polariton waveguides," Semiconductor Sci. Technol. **25**(3), 035003 (2010).
3. Y. S. Kang, S. B. Kim, Y. D. Chung, and J. Kim, "Optical coupling analysis of dual-waveguide structure for monolithic integration of photonic devices," IEEE Photon. Technol. Lett. **17**(11), 2304–2306 (2005).
4. Y. Kwon, J. Choe, J. Kim, K. Kim, K. Choi, B. Choi, and H. Yun, "Fabrication of 40 Gb/s front-end optical receivers using spot-size converter integrated waveguide photodiodes," ETRI J. **27**(5), 484–490 (2005).
5. I. Moerman and P. P. Van Daele, "A review on fabrication technologies for the monolithic integration of tapers with III-V semiconductor devices," IEEE J. Sel. Top. Quantum Electron. **3**(6), 1308–1320 (1997).
6. H. Yamazaki, K. Kudo, T. Sasaki, and J. Sasaki, "1.3-μm spot-size-converter integrated laser diodes fabricated by narrow-stripe selective MOVPE," IEEE J. Sel. Top. Quantum Electron. **3**(6), 1392–1398 (1998).
7. J. Stulemeijer, A. F. Bakker, I. Moerman, F. H. Groen, and M. K. Smit, "Efficient InP-based integrable spot-size converter," in *Integrated Photonics Research* (Optical Society of America, 1998).
8. H.-G. Bach, A. Beling, and G. G. Mekonnen, "Design and fabrication of 60-Gb/s InP-based monolithic photoreceiver OEICs and modules," IEEE J. Sel. Top. Quantum Electron. **8**(6), 1445–1450 (2002).
9. J. Wei, F. Xia, and S. R. Forrest, "A high-responsivity high-bandwidth asymmetric twin-waveguide coupled InGaAs-InP-InAlAs avalanche photodiode," IEEE Photon. Technol. Lett. **14**(11), 1590–1592 (2002).
10. T. Duthel, C. R. S. Fludger, J. Geyer, and C. Schulien, "Impact of polarisation dependent loss on coherent POLMUX-NRZ-DQPSK," in *2008 Conference on Optical Fiber Communication* (IEEE, 2008).
11. J. W. Bae, W. Zhao, J. H. Jang, I. Adesida, A. Lepore, M. Kwakernaak, and J. H. Abeles, "Characterization of sidewall roughness of InP/InGaAsP etched using inductively coupled plasma for low loss optical waveguide applications," J. Vac. Sci. Technol. B **21**(6), 2888 (2003).
12. F. Xia, J. K. Thomson, M. R. Gokhale, P. V. Studenkov, J. Wei, W. Lin, and S. R. Forrest, "An asymmetric twin-waveguide high-bandwidth photodiode using a lateral taper coupler," IEEE Photon. Technol. Lett. **13**(8), 845–847 (2001).

#196016 - $15.00 USD Received 19 Aug 2013; revised 6 Nov 2013; accepted 20 Nov 2013; published 2 Dec 2013

1. Introduction

Increasing requirement of internet data capacity drives optical communication to adopt sophisticated transmission techniques such as quadrature phase shift keying, coherent optical orthogonal frequency division multiplexing, and quadrature amplitude modulation, etc. Such techniques require a coherent receiver to convert optical signal into electric signal. An optical hybrid and two balanced photodetectors (PD) are integrated to form a single polarization coherent receiver. For 100 Gbps dual-polarization QPSK receiver, one polarization beam splitter, two optical hybrids, and four balanced PDs are required [1]. Therefore, integration of planar lightwave circuit (PLC) and PDs becomes more important.

Spot-size converter (SSC) is widely used for enhanced coupling efficiency in many semiconductor optical devices such as laser diodes [2], modulators [3], and PDs [4]. SSC in a PD has the role of transferring the relatively large launched beam to the absorbing mesa with small cross section. Tapers provide gradual change in the effective index of SSC, and its structure is mainly classified in lateral and vertical type [5]. Vertical tapers require gradual change of layer thickness that can be implemented through either selective area growth [6], diffusion-limited etching [7], or photolithography with moving mask, etc [8]. On the other hand, lateral tapers have advantage of simple fabrication through standard semiconductor process of photolithography and etching [4, 9].

Due to the large refractive indices of thin semiconductor materials that PD consists of, the cross section of the waveguide is not square but flat rectangle in general, which is different from the square waveguide of silica PLC. Therefore the shape of the waveguide mode is different in TE- and TM-polarization, and the propagation behavior between the two polarization is inevitably different. If the different propagation results in different opto-electric conversion efficiency, the PD would have polarization dependent loss (PDL). Considering that the polarization of signal through optical fiber continuously rotates, PDL should be kept as small as possible to suppress additional penalty in optical transmission link [10].

In this study, we optimized the design of SSC for low PDL through 3D finite-difference beam propagation method (BPM) simulation, and confirmed the optimization by measuring PDL of the fabricated devices.

2. Device design

We designed waveguide PD with integrated SSC composed of dual tapers and diluted waveguide as in Fig. 1. In order to apply conventional semiconductor processes of stepper and dry etching, lateral tapers were adopted. Diluted waveguide is for high coupling efficiency with cleaved single mode fiber (SMF) without focusing elements. An InGaAsP layer is located between absorber and upper taper as an *n*-type contact and index matching layer.

Table 1 shows materials and their refractive indices at 1.55μm used in analyzing the PD structure of Fig. 1. InP is used as cladding and thick low index layers in diluted waveguide. $In_{0.89}Ga_{0.11}As_{0.23}P_{0.77}$ (1.05Q, λ_g=1.05μm) is thin high index material in diluted waveguide. $In_{0.82}Ga_{0.18}As_{0.38}P_{0.62}$ (1.15Q, λ_g=1.15μm) is grown for the upper and lower tapers. $In_{0.76}Ga_{0.24}As_{0.5}P_{0.5}$ (1.24Q, λ_g=1.24μm) is located between taper and InGaAs absorber, and plays the role of index matching and *n*-contact layer. $In_{0.53}Ga_{0.47}As$ is material for absorbing 1.55μm light and *p*-contact. The effect of doping upon the refractive index was not considered for the following analysis.

Listed in Table 2 are physical dimensions of each elements of SSC. Diluted waveguide is 3.6 μm-thick and 790 μm-long. Its width is 9 μm at the facet and reduces to 6 μm just before the absorber. Lower taper has length of 750 μm, and its width increases from 1 μm at its tip to 4 μm. Upper taper is 250 μm-long, and gets wider from 0.5 to 2 μm as approaching to absorber. The thicknesses of 1.24Q matching layer and InGaAs absorbing layer are also fixed to 0.2 and

#196016 - $15.00 USD Received 19 Aug 2013; revised 6 Nov 2013; accepted 20 Nov 2013; published 2 Dec 2013

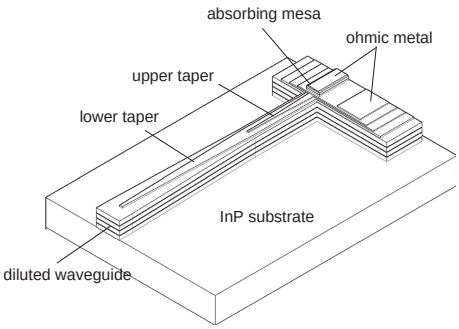

Fig. 1. Structure of the device investigated in this study. SSC is composed of two lateral tapers and diluted waveguide.

Table 1. Refractive indices and roles of the materials used in simulation.

material	refractive index		purpose
	n	k	
$In_{0.53}Ga_{0.47}As$	3.56	0.086	absorber, p-contact
1.24Q	3.35	0	n-contact, index matching
1.15Q	3.30	0	lower and upper taper
1.05Q	3.25	0	core of diluted waveguide
InP	3.17	0	substrate, clad of diluted waveguide, p-clad

Table 2. Physical dimensions of each elements of SSC.

	diluted waveguide	lower taper	upper taper
width	9 μm $\rightarrow$ 6 μm	1 μm $\rightarrow$ 4 μm	0.5 μm $\rightarrow$ 2 μm
length	790 μm	750 μm	250 μm
thickness	3.6 μm	variable	variable

0.43 μm, respectively. Three 1.05Q layers of 0.1 μm thickness are inserted in InP with 1 μm spacing to form the diluted waveguide. The width and length of the InGaAs absorber are 5 and 20 μm, respectively. Optimization of the SSC was performed through BPM simulation by varying only the thicknesses of the tapers.

Figure 2 shows the evolution of launched beam (λ=1.55 μm) which is (a) TE- and (b) TM-polarized. The mode of an SMF was chosen as the launch field, assuming that fabricated device would be butt-coupled with cleaved SMF without additional optical components. For both the polarizations, the beam that is launched on the cleaved diluted waveguide transfers to the lower and upper taper in sequence, and finally absorbed in the InGaAs mesa. But the shape of the beam evolution is quite different. While TE-polarized beam escapes from the diluted waveguide at the early stage of the lower taper, TM-polarized beam stays there until the upper taper appears. This difference may cause large PDL, but is not removed by changing the simulation parameters in Table 2. Therefore a quantitative analysis is necessary to estimate PDL.

In order to estimate PDL for a given combination of tapers' thicknesses, responsivity of the PD was calculated for each polarization. BPM simulation gives the change in total optical power

#196016 - $15.00 USD Received 19 Aug 2013; revised 6 Nov 2013; accepted 20 Nov 2013; published 2 Dec 2013

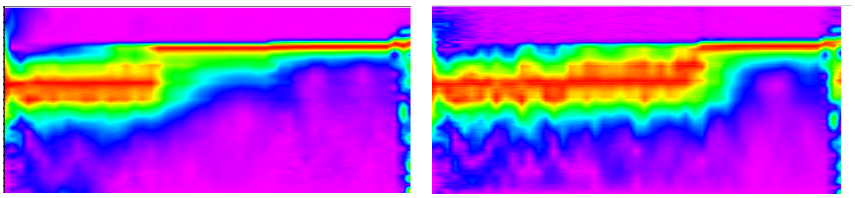

(a) (b)

Fig. 2. Evolution of launched beam into PD when the beam is (a) TE- and (b) TM-polarized. When TE-polarized, the launched beam escapes from the diluted waveguide at the early stage of the lower taper. On the other hand, TM-polarized beam stays in the diluted waveguide until the upper taper appears.

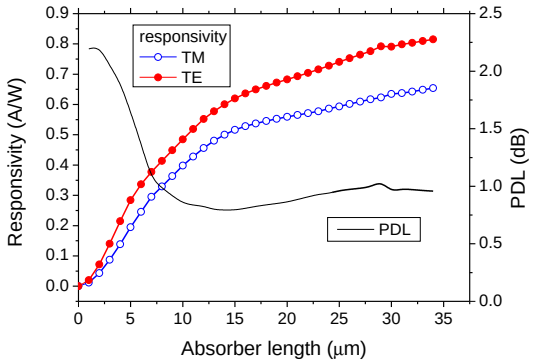

Fig. 3. Calculated responsivity as a function of absorber length (left axis). In this case responsivity depends strongly on the polarization of incident beam. PDL is obtained from the two responsivity curves (right axis). PDL is saturated when the absorber is longer than 10 μm.

during the beam propagation. Its cause can be either radiation or absorption. The beam scatters when it meets the absorbing mesa, as in Fig. 2, but most of the scattered power is also included in the total power because of the wide computation region below the diluted waveguide. Thus in this analysis we assumed that absorption is the only origin of the total optical power reduction after the beam reaches the absorbing mesa.

Once the difference in total optical power at both ends of the absorbing mesa is calculated, responsivity in A/W is easily induced from the following equation:

$$\begin{aligned} R &= \frac{I_{\text{photo}}}{P_{\text{input}}} = \frac{P_{\text{abs}}}{P_{\text{input}}}\frac{q\lambda}{hc} \simeq \frac{P_{\text{abs}}}{P_{\text{input}}}\frac{\lambda(\mu\text{m})}{1.24}(\text{A/W}) \\ &= 1.25 \times \frac{P_{\text{abs}}}{P_{\text{input}}}(\text{A/W}) \qquad \text{if } \lambda = 1.55\ \mu\text{m} \end{aligned} \tag{1}$$

where I_{photo}, P_{input}, P_{abs}, q, h, c, and λ are photocurrent, optical input power, absorbed optical power, electric charge, Planck constant, speed of light, and wavelength of the input light, respectively. Figure 3 shows calculated responsivity as functions of absorber length when the thicknesses of the lower and upper taper are 0.43 and 0.13 μm, respectively. Responsivity increases steeply with absorber length until 15 μm, and the slope becomes relatively flat at longer length than that. Over the range of length calculated, TE-polarized beam has larger responsivity than TM-polarized. PDL can be induced using the responsivity of each polarization from its

#196016 - $15.00 USD Received 19 Aug 2013; revised 6 Nov 2013; accepted 20 Nov 2013; published 2 Dec 2013

definition:

$$\mathrm{PDL(dB)} = 10\left|\log\frac{R_{TE}}{R_{TM}}\right|, \tag{2}$$

and is also plotted in Fig. 3. When absorber is short, responsivity is small for both the polarizations, and PDL is very large. As absorber gets longer than 10 μm, PDL reduces to a saturated value about 1 dB. In this report 20-μm-long absorber was chosen for both the simulation and device fabrication.

To optimize SSC for small PDL, this analysis was repeated for various combinations of tapers. Firstly, contour map of responsivity at 1.55 μm was made for each polarization, as is shown in Fig. 4. The combinations of tapers for the calculation were chosen such that the total

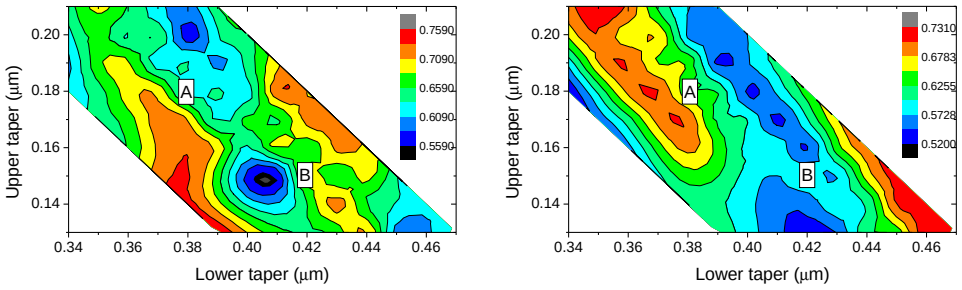

Fig. 4. Contour map of estimated responsivity in (a) TE- and (b) TM-polarization. Responsivity varies from 0.56 to 0.76 A/W in TE-polarization, and from 0.52 to 0.73 A/W in TM-polarization. Although maximum and minimum values of the responsivity are similar for both the polarizations, the contour maps are quite different from each other.

thickness of the two tapers is between 0.52 and 0.60 μm. Although the variation in thickness is smaller than 0.08 μm, responsivity varies widely. Responsivity varies from 0.56 to 0.76 A/W in TE-polarization, and 0.52 to 0.73 A/W in TM-polarization. Thus the two polarizations have similar maximum and minimum responsivity. But the responsivity contour map is quite different, as can be seen in Fig. 4(a) and (b), and it will produce large non-uniformity in the distribution of PDL. For example, combination A (upper taper = 0.18 μm, lower taper = 0.38 μm) is expected to show responsivity of 0.61 and 0.63 A/W in TE and TM polarization, respectively. On the other hand, responsivity of design B (upper taper = 0.15 μm, lower taper = 0.42 μm) in TE and TM polarization is 0.60 and 0.71 A/W. Thus, expected PDL value of design A and B is 0.14 and 0.73 dB.

Figure 5 is the contour plot of PDL obtained using Fig. 4. PDL has values from 0.0 to 1.1 dB, and there is a region with low PDL. As some taper combinations have low PDL and insufficient responsivity, optimum SSC should be determined from both Fig. 4 and Fig. 5. Design A was chosen as the optimum design from Fig. 5 for device fabrication. It has advantages of not only low PDL and good responsivity, but also sufficient tolerance for etching process. Design B was chosen to be compared with the optimum design A. Devices of design B (PD-B) are expected to have larger PDL and smaller responsivity than the devices of design A (PD-A). In addition, large variance in PDL is expected among PD-B devices, judging from the high density of the contour lines near the point.

3. Device fabrication

Epilayers were prepared for the device fabrication by metallorganic chemical vapor deposition. Absorbing mesa, *n*-contact region, upper taper, lower taper, and diluted waveguide were

#196016 - $15.00 USD Received 19 Aug 2013; revised 6 Nov 2013; accepted 20 Nov 2013; published 2 Dec 2013

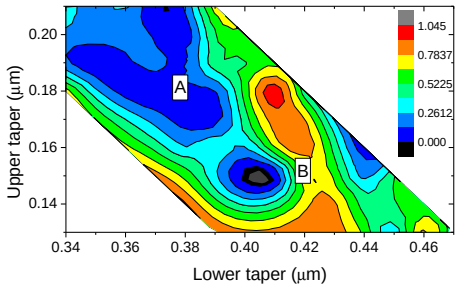

Fig. 5. Contour plot of calculated PDL. PDL changes from 0.0 to 1.1 dB, and there exist wide region with low PDL. Combination of tapers A was chosen as the optimum design for device fabrication. For the comparison, combination B was also chosen.

sequentially formed by etching processes. In this study, 1.15Q single layer was grown for the two tapers, and each taper was formed through reactive ion etching. As the thickness control of the tapers is critical in the fabrication process, each taper was carefully etched. Surface profiler analysis showed that the etch depth of the tapers was close to the target depth within 50 Å. The lower taper formation was finalized by slight wet etching using selective etchant (H_3PO_4:H_2O_2:H_2O=1:1:10). Polyimide was used to passivate the sidewall of etched mesa. Anti-reflection coating was deposited on the input facet after cleaved.

4. Device characterization

The dark current level of the fabricated device was about 10 nA at -3 V. The coupling function of SSC was assessed by measuring the alignment tolerance and responsivity. A source-measure unit (SMU, Keithley 236) supplied bias to a PD mounted on a vacuum chuck. A motorized polarization controller (Agilent 11896A) was connected to the output of a DFB LD ($\lambda = 1.55$ μm) in order to manipulate polarization of the incident beam. The output of the polarization controller was transferred to PD devices via a cleaved SMF. The gap between the SMF and PD was about 2 μm. A stepping-motor positioner moved the SMF in either horizontal or vertical direction for alignment or sweep.

The maximum responsivity of PD-A and PD-B was 0.46 and 0.32 A/W, respectively, at optimum SMF position and beam polarization. The low responsivity compared with the values expected in Fig. 4 is seemed to be due to the simple assumption for obtaining absorbed power from total power change. The assumption may cause error when there exists radiation or scattering that is not included in the simulation. While the simulation model assumes that SMF is in contact with PD, there is a gap between SMF and PD. The beam from the SMF diverges with angle so that the simulation underestimated the radiation loss near the input facet of the PD. The radiated portion can be large toward the substrate because of the weak guiding of the diluted waveguide. Thick ridge of the diluted waveguide was formed through consecutive three RIE processes, which caused steps and roughness at the sidewall resulting in scattering loss [11]. For comparison, we also measured responsivity with a tapered fiber ($R = 10$ μm). Responsivity over 0.7 A/W was obtained that is similar level reported in other literature [12].

Figure 6 is responsivity data of PD-A as a function of SMF position, measured at every 0.5 μm. Under the measurement condition 1 dB alignment tolerance is 4.5 and 5.0 μm in vertical and horizontal direction, respectively. The shape of the photocurrent profile was nearly unchanged when the polarization of the input beam changed. PD-B showed similar alignment tolerance behavior.

The PDL characteristics of the fabricated devices was measured using responsivity measure-

#196016 - $15.00 USD Received 19 Aug 2013; revised 6 Nov 2013; accepted 20 Nov 2013; published 2 Dec 2013

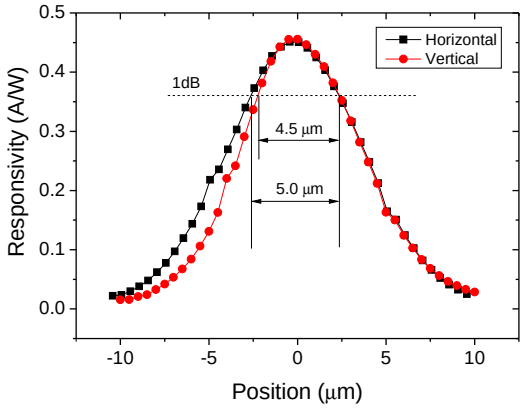

Fig. 6. Dependence of responsivity upon the position of cleaved SMF. 1 dB alignment tolerance is 4.5μm and and 5.0 μm in vertical and horizontal direction, respectively. At the optimum position the responsivity is 0.46 A/W.

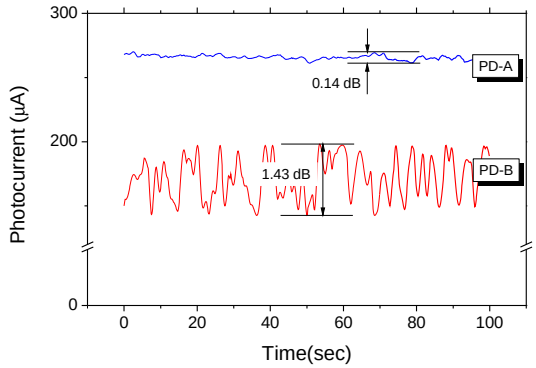

Fig. 7. Photocurrent fluctuation with the change in the polarization of incident beam. PD-B, the device with unoptimized SSC, shows PDL of 1.43 dB. On the other hand, PD-A has optimized SSC and its photocurrent fluctuation is so small that PDL is as low as 0.14 dB.

ment setup with the motorized polarization controller in operation. While the polarization moved along an arbitrary path on the Poincaré sphere, PD's photocurrent was measured every 100 msec for 100 sec. Photocurrent fluctuated with time, and PDL was determined from the maximum and minimum values by eq. (2)

Measured photocurrents of PD-A and PD-B under varying polarization are shown in Fig. 7. PD-B shows large photocurrent fluctuation which corresponds to PDL of 1.43 dB. On the other hand, PDL of PD-A is as small as 0.14 dB. Statistical property of PDL is also quite different between the two devices. When 34 devices were measured, PDL of PD-A showed mean and standard deviation of 0.15 and 0.11 dB, respectively. This small PDL is consistent with the simulation result. Considering that the point A in Fig. 5 is located in a relatively flat region, a variation in etch depth does not affect much unless it is larger than $\sim$100 Å, suggesting that the optimized SSC structure is applicable to commercial fabrication requiring high yield. For PD-B devices, mean value of PDL was 1.22 dB, and its standard deviation was 0.68 dB. The difference between measured and expected PDL of PD-B is somewhat large value of 0.49 dB,

#196016 - $15.00 USD Received 19 Aug 2013; revised 6 Nov 2013; accepted 20 Nov 2013; published 2 Dec 2013

which is attributed to dimension-sensitive design of PD-B. Considering that effective index of any waveguide depends on its width as well as thickness, PD-B will also be strongly dependent on the widths of the tapers. The widths of the tapers are deviated from the original layout by over- or under-development in photolithography, and undercut formation during the selective wet etching of the lower taper. Although PD-A also suffers the deviation in widths of its tapers, it shows PDL similar to the simulated result because it was designed to be immune to such influence.

5. Conclusion

SSC with dual lateral tapers was optimized for small PDL of waveguide PD using BPM simulation. It was found that proper thicknesses of the tapers are very important for good responsivity and PDL characteristics, and there is an optimum condition that also provides sufficient tolerance for etching process. Devices were fabricated according to the optimized structure, and the resultant devices confirmed our analysis with their small PDL and standard deviation. Devices with unoptimized SSC were also made, and they showed much worse PDL characteristics.

Acknowledgment

This work was supported by the IT R&D program of MKE/KIAT(2010-TD-200408-001, Coherent transmitter and receiver development), Republic of Korea.

#196016 - $15.00 USD Received 19 Aug 2013; revised 6 Nov 2013; accepted 20 Nov 2013; published 2 Dec 2013